ARTICLE OPEN

Spontaneous emergence of Josephson junctions in homogeneous rings of single-crystal Sr_2RuO_4

Yuuki Yasui [1,6,7], Kaveh Lahabi [2,7], Victor Fernández Becerra [3,4], Remko Fermin [2], Muhammad Shahbaz Anwar[1,5], Shingo Yonezawa [1], Takahito Terashima[1], Milorad V. Milošević[3], Jan Aarts [2] and Yoshiteru Maeno [1] ✉

The chiral p-wave order parameter in Sr_2RuO_4 would make it a special case amongst the unconventional superconductors. A consequence of this symmetry is the possible existence of superconducting domains of opposite chirality. At the boundary of such domains, the locally suppressed condensate can produce an intrinsic Josephson junction. Here, we provide evidence of such junctions using mesoscopic rings, structured from Sr_2RuO_4 single crystals. Our order parameter simulations predict such rings to host stable domain walls across their arms. This is verified with transport experiments on loops, with a sharp transition at 1.5 K, which show distinct critical current oscillations with periodicity corresponding to the flux quantum. In contrast, loops with broadened transitions at around 3 K are void of such junctions and show standard Little–Parks oscillations. Our analysis demonstrates the junctions are of intrinsic origin and makes a compelling case for the existence of superconducting domains.

INTRODUCTION

Sr_2RuO_4 stands out among the unconventional superconductors as one of the few materials with a chiral order parameter[1,2]. The tetragonal crystal structure allows five unitary representations for a p-wave pairing symmetry[1,3]. One of these is the chiral order parameter, of the form $k_x \pm ik_y$, which is strongly suggested by muon spin relaxation[4] and high-resolution polar Kerr effect measurements[5]. Very recently, nuclear magnetic resonance experiments demonstrated that the d-vector is not parallel to the c-axis and suggested possible chiral d-wave states[6,7]. Such chiral states are attracting renewed attention due to the possibility of hosting Majorana bound states, which in turn are of interest for topological quantum computing[8–10]. A key property of the chiral state is its double degeneracy in the orbital degree of freedom, with important consequences such as the existence of superconducting domains of different chirality and a spontaneous edge current. The major problem plaguing our understanding of Sr_2RuO_4[11] is that, although the chiral state seems probable, domains or edge currents have not been observed directly. Indications for their existence, however, have been found in transport experiments, which utilise Ru inclusions to form proximity junctions between Sr_2RuO_4 and a conventional s-wave superconductor[12,13]. A complication in the physics of Sr_2RuO_4 is that breaking of the tetragonal crystal symmetry due to Ru inclusions or a uniaxial strain can induce a different superconducting state with an enhanced superconducting transition temperature $T_c \approx 3$ K[14,15]. Recent experiments suggest that this so-called 3-K phase may exhibit a non-chiral state with a single-component order parameter[16,17]. In this paper, we refer to the multi-component phase with T_c of around 1.5 K, associated with the pure bulk limit, as the "intrinsic phase" and the possible single-component phase, characterised by $T_c \approx 3$ K, as the "extrinsic phase".

The vast majority of experiments in the past two decades have been limited to bulk crystals, typically hundreds of microns in dimension. This is partly due to the unavailability of superconducting Sr_2RuO_4 films. The chiral domains, however, are expected to be no more than a few microns in size[5,13]. Moreover, the time-dependent switching noise observed in transport measurements suggests the domains are mobile[12,13]. We note here that the role of chiral domains resulting in hysteretic behaviour has been discussed in the Bi-Ni bilayer system[18]. The arbitrary configuration of the domains introduces an element of uncertainty. On the other hand, the energy cost associated with a chiral-domain wall (ChDW) grows per area[19]. It has been recently discussed that mesoscopic samples made of chiral p-wave superconductors could host multichiral states[20,21], where the two $k_x \pm ik_y$ chiral components are divided into superconducting domains, separated by ChDWs. This makes mesoscopic structures a promising platform to verify and potentially control the domains. Another interesting aspect of a ChDW is that it can act as a Josephson junction[19] due to the local suppression of the order parameter, as schematically shown in Fig. 1a.

Here, we present results of transport measurements on mesoscopic rings of Sr_2RuO_4, prepared by focused ion beam (FIB) milling of single crystals. Homogeneous structures, characterised by a sharp transition at around the intrinsic T_c of 1.5 K, show distinct critical current oscillations—similar to that of the classical DC superconducting quantum interference device (SQUID), consisting of two artificially prepared Josephson junctions. Despite the absence of conventional weak links, the interference pattern appears over the full temperature range below T_c while maintaining its overall shape. In contrast, the SQUID oscillations are entirely absent in rings that are in the extrinsic phase. These systems behave as standard superconducting loops: they exhibit the conventional Little–Parks (LP)[22] T_c oscillations, which can only be observed near the resistive

[1]Department of Physics, Graduate School of Science, Kyoto University, Kyoto 606-8502, Japan. [2]Huygens—Kamerlingh Onnes Laboratory, Leiden Institute of Physics, Leiden University, P.O. Box 9504, 2300 RA Leiden, The Netherlands. [3]Department of Physics, University of Antwerp, Groenenborgerlaan 171, 2020 Antwerp, Belgium. [4]International Research Centre Magtop, Institute of Physics, Polish Academy of Sciences, Aleja Lotników 32/46, 02-668 Warsaw, Poland. [5]Department of Materials Science and Metallurgy, University of Cambridge, 27 Charles Babbage Road, Cambridge CB3 0FS, UK. [6]Present address: RIKEN Center for Emergent Matter Science, Wako, Saitama 351-0198, Japan. [7]These authors contributed equally: Yuuki Yasui, Kaveh Lahabi. ✉email: maeno@scphys.kyoto-u.ac.jp
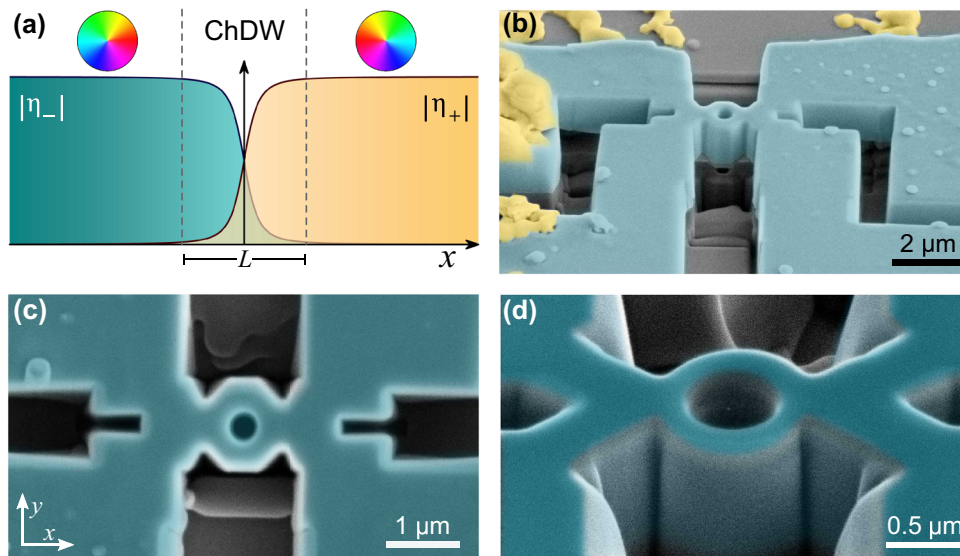
Fig. 1 Superconducting domain wall and the Sr₂RuO₄ microring. a Schematic of a chiral-domain wall (ChDW). η_- and η_+ represent the degenerate chiral states meeting at a ChDW. The colour wheels represent the orbital phase of the chiral components, which wind in opposite directions. The two chiral wavefunctions overlap over a finite length L. As they locally suppress each other, a Josephson junction is formed. **b** False-colour scanning electron microscope (SEM) image of Ring A. The blue represents the Sr₂RuO₄ crystal, and the yellow represents silver paint used for making electrical contact. Close-up images of **c** Ring A and **d** Ring B. In both rings the outer radius is around 0.55 μm while the inner radius of Ring B ($r_{in} = 0.3$ μm) is slightly larger than that of Ring A $r_{in} = 0.23 \pm 0.04$ μm. Each ring is connected to four transport leads and is sculpted out of a single crystal (around 0.7 μm thick) by a Ga⁺ focused ion beam.
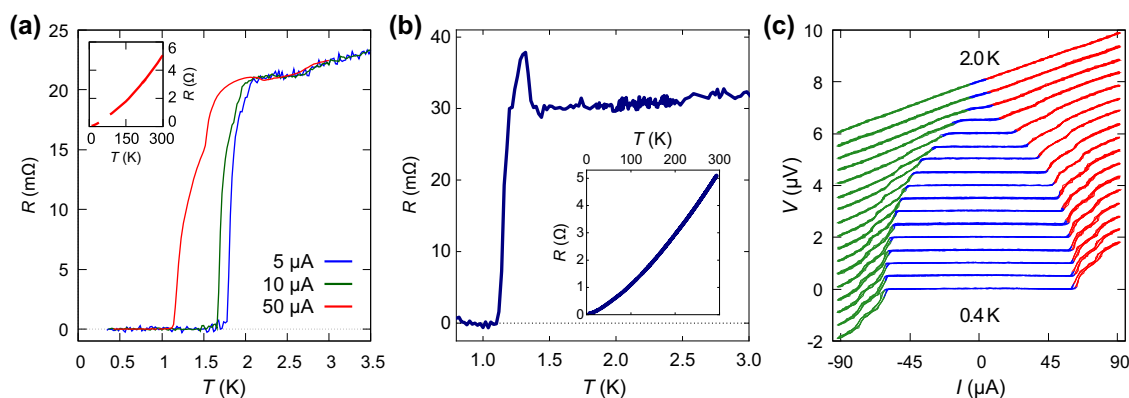

Fig. 2 Basic properties of the Sr₂RuO₄ microrings. Resistance as a function of temperature $R(T)$ for **a** Ring A and **b** Ring B. **a** presents data for various measurement currents, and **b** was measured using 10 μA. The insets show the $R(T)$ over a wider temperature range. Both rings exhibit highly metallic behaviour with residual resistivity ratio of 238 for Ring A and 177 for Ring B. **c** Current–voltage characteristics $V(I)$ of Ring A at various temperatures. The colours represent different voltage regions: $V < -0.1$ μV (green), $-0.1 < V < 0.1$ μV (blue), and 0.1 μV $< V$ (red).

transition[21]. We also present calculations on the possible chiral-domain configurations for a p-wave superconducting ring, using the Ginzburg–Landau (GL) formalism. Experiments and calculations together make a convincing case for the existence of ChDWs in the intrinsic phase of Sr₂RuO₄.

RESULTS

Basic transport properties of single-crystal microrings

Single crystals of Sr₂RuO₄ were grown with the floating zone method[23] and structured into microrings using Ga-based FIB etching. Figure 1b–d shows scanning electron microscope (SEM) images of Rings A and B. The inner and outer radii of Ring A are $r_{in} \approx 0.21$ μm and $r_{out} = 0.55$ μm, respectively. Similar dimensions are used in Ring B: $r_{in} = 0.3$ μm and $r_{out} = 0.54$ μm. Both crystals have a thickness of around 0.7 μm.

The temperature-dependent resistance $R(T)$ of both rings (presented in Fig. 2a, b) shows sharp superconducting transitions

similar to that of bulk Sr₂RuO₄. The apparent enhancement of the resistance just above T_c in Fig. 2b could be attributed to changes in the current path[24]. The high quality of the sample is also evident by their particularly high residual resistivity ratio; RRR = R (300 K)/R(3 K) = 238 for Ring A and RRR = 177 for Ring B. To demonstrate that FIB milling does not alter the intrinsic characteristics of Sr₂RuO₄, we compare the $R(T)$ of Ring A with the one measured before milling the crystal in Supplementary Fig. 1, which shows that T_c and the overall transport properties remain unchanged under structuring. Figure 2c shows the typical current–voltage $V(I)$ behaviour at different temperatures. For both rings, the $V(I)$ measurements exhibit negligibly small hysteresis even at temperatures far below T_c.

Insights from theoretical simulations

Before presenting the results of transport measurements under a magnetic field, we examine the expected chiral-domain configurations in our structure. This is accomplished by performing detailed
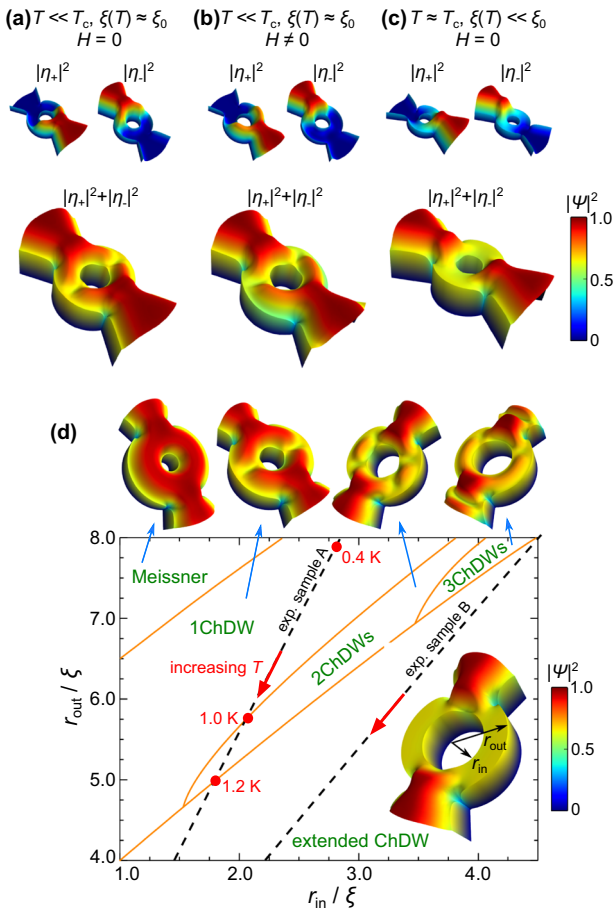
(a) $T \ll T_c, \xi(T) \approx \xi_0$
$H = 0$

$|\eta_+|^2$ $|\eta_-|^2$

$|\eta_+|^2 + |\eta_-|^2$

(b) $T \ll T_c, \xi(T) \approx \xi_0$
$H \neq 0$

$|\eta_+|^2$ $|\eta_-|^2$

$|\eta_+|^2 + |\eta_-|^2$

(c) $T \approx T_c, \xi(T) \ll \xi_0$
$H = 0$

$|\eta_+|^2$ $|\eta_-|^2$

$|\eta_+|^2 + |\eta_-|^2$

$|\Psi|^2$
1.0
0.5
0

(d)

r_{out}/ξ

8.0

7.0   Meissner

1ChDW   exp. sample A   0.4 K

increasing T   2ChDWs   exp. sample B   3ChDWs

6.0   1.0 K

$|\Psi|^2$
1.0
0.5
0

r_{out}
r_{in}

5.0   1.2 K

extended ChDW

4.0

1.0   2.0   3.0   4.0
r_{in}/ξ

Fig. 3 Simulated least-energy-state configurations of chiral *p*-wave microrings with nanostructured transport leads. a State at a temperature much below T_c without magnetic field (specifically, $T \approx 0.78$K, $r_{in} = 2.5\xi$, and $r_{out} = 6.8\xi$). **b** State at the same temperature as (**a**) but with axial magnetic field. **c** State at a temperature close to T_c in zero magnetic field (specifically, $T \approx 1.45$K, $r_{in} = 1.3\xi$, and $r_{out} = 3.6\xi$). These states contain ChDWs that act as weak links of a SQUID. The colour maps represent the Cooper-pair density $|\Psi|^2$. In the panels (**a–c**), the inner r_{in} and outer r_{out} radii correspond to those of Rings A and B. The upper halves of the panels show the Cooper-pair density for each chiral component $|\eta_\pm|$ of the corresponding states, for which the overall order parameter is expressed by $\Psi = \eta_+ k_+ + \eta_- k_-$. **d** $\left(\frac{r_{in}}{\xi(T)}, \frac{r_{out}}{\xi(T)}\right)$. Phase diagram in the absence of a magnetic field. For a wider ring arm, the "Meissner" state without ChDW is more stable; for a narrower ring arm, the extended ChDW state is expected. The dashed line shows the evolution of the least-energy states with increasing temperature according to the actual parameters of Ring A.

time-dependent GL simulations, under the assumption of a chiral *p*-wave order parameter, for microrings with nanostructured transport leads (similar to the one used in our experiments). The simulations show that the ring can host a mono-chiral-domain or a multi-domain state, depending on the parameters $\frac{r_{in}}{\xi(T)}$ and $\frac{r_{out}}{\xi(T)}$, which correspond to the inner and outer radii of the ring, scaled by the temperature-dependent coherence length $\xi(T) = \xi(T = 0)\frac{\sqrt{1-t^4}}{1-t^2}$[25,26], where $t = \frac{T}{T_c}$, with $T_c \approx 1.75$ K for Ring A and $T_c \approx 1.3$ K for Ring B (shown in Fig. 2a, b). Based on our critical field measurements, we estimate $\xi(T = 0) \sim 66$ nm, which is the same as the bulk value for Sr_2RuO_4. Figure 3a shows the simulated Cooper-pair density $|\Psi|^2$ of Ring A far below T_c, obtained by setting $\frac{r_{in}}{\xi(T)} = 2.5$ and $\frac{r_{out}}{\xi(T)} = 6.8$ (corresponding to $T \lesssim 0.5T_c$ in our measurements). This state contains two

distinct chiral domains, separated by a pair of ChDW. Within the domain wall the order parameter is reduced to about half of its original amplitude in the banks on each side, resulting in the formation of two parallel Josephson weak links. While the suppressed order parameter is unfavourable in terms of the condensation energy, the formation of such ChDW is favoured by the second term of the free energy in Supplementary Eq. (S11). Since the order parameter is suppressed at the sample edge, the second term gains importance with reducing sample size and may further enhance an inhomogeneous order-parameter state with a ChDW. The ChDW region extends over a length of the order of ξ. As shown in Fig. 3b, the presence of a magnetic field along the ring axis makes the positions of the ChDWs shift away from the middle of the arms since one of the chiral components is favoured by the magnetic field. The ChDWs, however, remain in the arms of the ring due to the strong pinning by the restricted dimensions.

Figure 3c shows the calculated chiral-domain configuration for Ring B, which also applies to Ring A at temperatures near T_c. This is obtained by setting $\frac{r_{in}}{\xi(T)} = 1.3$ and $\frac{r_{out}}{\xi(T)} = 3.6$ (corresponding to $T \approx 1.45$ K for Ring A). As the arms of the ring are now considerably narrower on the scale of $\xi(T)$, the contribution of the edge regions dominates the configuration of the order parameter. As a consequence, it becomes energetically favourable for the two chiral components to coexist over the entire ring. This state also produces a pair of parallel weak links due to the suppression of the order parameter $|\Psi|$, which extend over the arms of the rings. Figure 3d presents a phase diagram of the lowest energy states, calculated for various $\left(\frac{r_{in}}{\xi(T)}, \frac{r_{out}}{\xi(T)}\right)$. Amongst these, mono-domain "Meissner" state can be stabilised by increasing the r_{out}/r_{in} ratio. In this state, the arms of the ring are unable to provide effective pinning of ChDWs. This scenario is explored in Supplementary Note 4 and Supplementary Fig. 5, where a ring with relatively wide arms (Ring E) approaches the mono-domain state at low temperatures. The evolution of the equilibrium domain configuration as a function of temperature for Rings A and B are represented by the dashed lines in Fig. 3d. This suggests that the rings are in one of the domain states shown in Fig. 3a and c at all temperatures below T_c, except in a narrow range around 1–1.2 K, where additional domain walls could appear in Ring A. As a general finding, our GL calculations show that ChDWs could spontaneously emerge in our mesoscopic rings and behave as stable Josephson junctions over a broad temperature range, resulting in a DC SQUID of intrinsic origin. The change of chirality across such junctions and its influence on their transport characteristics remain open questions and are worthy of further studies. Note that the GL formalisms for chiral *p*-wave and chiral *d*-wave superconductors have analogous form, and the segregation of chiral domains as discussed above is applicable to both cases.

Critical current oscillations

We examined the supercurrent interference of the rings by measuring I_c at each magnetic field H. The results are presented in Fig. 4, where we observe the same behaviour in both Rings A and B. Figure 4a, b shows the I_c of Ring A, measured for positive (I_{c+}) and at negative (I_{c-}) bias currents, taken at temperatures deep inside the superconducting state and close to T_c, respectively. For both temperatures, we observe distinct critical current oscillations, with the period corresponding to the fluxoid quantisation over the ring area. This interference pattern corresponds to that of a DC SQUID with a pair of parallel Josephson junctions. The junctions would also need to be symmetric each other; an imbalance in I_c could not produce the cusp-shaped minima of the patterns. The figure also shows $-I_{c-}(-H)$ overlaid on its time-reversed counterpart, $+I_{c+}(H)$. Figure 4c shows that the same SQUID oscillations appear in Ring B, only with a slightly smaller period (consistent with its slightly larger inner radius). The oscillations emerge
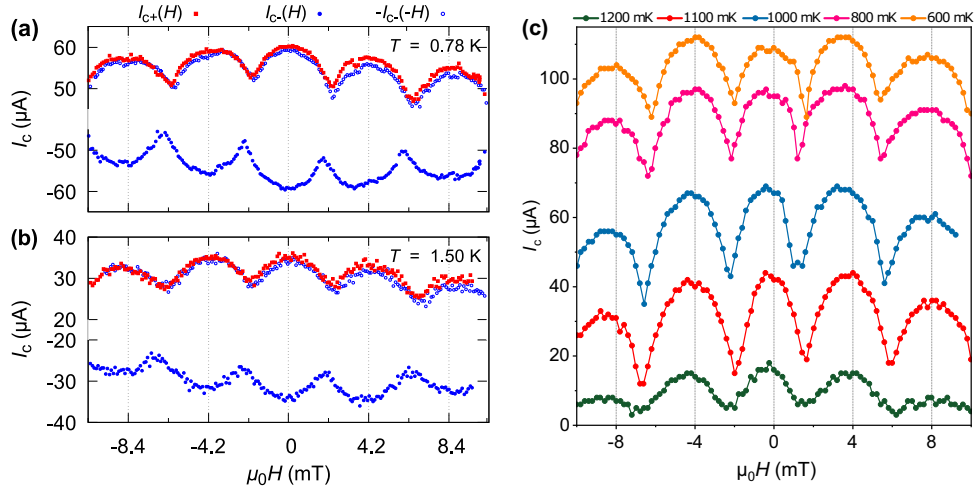
Fig. 4 SQUID oscillations observed in the Sr$_2$RuO$_4$ microrings. a Critical current as a function of magnetic field $I_c(H)$ of Ring A measured at 0.78 and 1.50 K. The open blue circles show time-reversed critical current. **c** I_c oscillations in Ring B over a wide range of temperatures. The I_c values were obtained from $I(V)$ measurements at each magnetic field. The rings were heated up to above 5 K between each magnetic field.

spontaneously at the onset of superconductivity and continue down to $T \ll T_c$. More importantly, we find that the patterns are not distorted, despite the substantial variations in $I_c(T)$ and $\xi(T)$.

It is worth noting that, unlike the polar Kerr experiments, we find field cooling and zero-field cooling of the samples to yield the same results in our measurements. This, however, is to be expected in mesoscopic structures, where domain walls are strongly pinned to the confined regions in order to lower the free energy of the system (see Supplementary Note 2 and Supplementary Fig. 2 for more details). Such pinning mechanism is absent in the polar Kerr experiments, which are performed on bulk crystals[5].

To demonstrate the robustness of the SQUID behaviour further, in Fig. 5a, b, we plot the magnetoresistance of Ring A, produced by the I_c oscillations over a wide range of temperatures. These are measured by applying a constant DC current $\pm I$ while sweeping the magnetic field H along the ring axis. Here, the resistance R is defined by the average of two voltages before and after current reversal at each magnetic field; $R = [V(I) - V(-I)]/2I$. When the measurement current exceeds the critical current $I_c(H)$, the system is driven out of the zero-voltage regime of the $V(I)$ and produces a finite resistance. Combining the results of a wide range of temperatures, Fig. 5a, b reveals that the SQUID oscillations emerge together with I_c at the onset of the superconducting transition. In Fig. 5c, d, we describe the shape of $R(H)$, where in some cases the peaks can appear to be split or broadened. This is clearly due to a slight difference in the values of $I_{c\pm}$, which causes the voltage peaks for $\pm I$ to appear asymmetrically. We observed a similar asymmetry in rings showing the LP effect[27].

The magnetovoltage and field-dependent $V(I)$ measurements are crucial in resolving an outstanding issue regarding previous reports of unconventional behaviour of Sr$_2$RuO$_4$ rings. Cai et al. have consistently observed magnetoresistance oscillations with unexpectedly large amplitude[28,29], very similar to the data presented in Fig. 5. The reported magnetoresistance oscillations are also stable over a wide range of temperatures and, in some cases, show small dips around $\Phi_0/2$. As Fig. 5 demonstrates, however, the averaged resistance R could produce a very similar effect even when there is no splitting of the peaks in the raw magnetovoltage signal.

T_c oscillations in rings with an extrinsic phase

We already mentioned that ChDWs can produce the observed $I_c(H)$ oscillations by acting as Josephson junctions. This should be

contrasted with the fluxoid-periodic behaviour of structures with a partial or full extrinsic phase, characterised by a noticeably broader transition which begins near 3 K (see Fig. 6e and Supplementary Fig. 4). We recently reported observations of the LP oscillations in such Sr$_2$RuO$_4$ microrings[27], and here we demonstrate that those are of a fundamentally different nature than the I_c oscillations discussed in this report. For this, we compare the data from Ring A with those of Ring C (sample B in ref.[27]), where the transition is considerably broader (Fig. 6e). This ring was prepared from a 2-μm-thick crystal with a T_c of 1.5 K. After microstructuring, however, the ring was found to have a higher T_c, with its transition already starting at 2.7 K. The magnetotransport measurements reveal that the ring itself is predominantly in the extrinsic phase, introduced by microstructuring (most likely due to a strain induced by FIB milling of the thick crystal). Compared to Rings A (RRR = 238) and B (RRR = 177), this structure has a smaller residual resistivity ratio RRR = 129. Nevertheless, the value of RRR is still substantial, indicating strong metallicity for Ring C. Figure 6a, b shows $R(H)$ for temperatures within the resistive-transitions of Rings A and C (taken 1.67 K and 2.3 K, respectively). In both cases we find fluxoid-periodic oscillations, which we compare with simulated LP oscillations (the red curves).

The change of the transition temperature due to the LP oscillations is given by[30]:

$$\frac{T_c(H) - T_c(0)}{T_c(0)} = -\left(\frac{\pi\xi(0)w\mu_0 H}{\sqrt{3}\Phi_0}\right)^2 - \frac{\xi^2(0)}{r_{in}r_{out}}\left(n - \frac{\pi\mu_0 H r_{in} r_{out}}{\Phi_0}\right)^2, \qquad (1)$$

where $\Phi_0 = h/2e$ is the flux quantum with the Planck constant h and the elementary charge e, and $w = r_{out} - r_{in}$ is the width of a ring arm. The first term represents the effect of the Meissner shielding, and the second term corresponds to fluxoid quantisation. To convert the change of the transition temperature to the resistance variation, we assume that the $R(T)$ curve does not change its shape under magnetic field and shifts horizontally by $\Delta T_c(H) = T_c(H) - T_c(0)$. For the simulations in Fig. 6a, b, we used $\xi(0) = 66$ nm, $2r_{in} = 0.55$ μm, $2r_{out} = 1.1$ μm for Ring A, and $2r_{in} = 0.7$ μm, $2r_{out} = 1.0$ μm for Ring C. Both the period and amplitude of the oscillations for Ring C agree with those of the simulation. We therefore consider these to be the LP oscillations, driven by variations in T_c. For Ring A, however, the oscillation amplitude is substantially larger than what T_c variations can produce. Such large-amplitude magnetoresistance is driven by the $I_c(H)$ oscillations instead. In Fig. 6c, d, we compare the $I_c(H)$ of both rings at lower temperatures. In contrast to Rings A and B, the SQUID
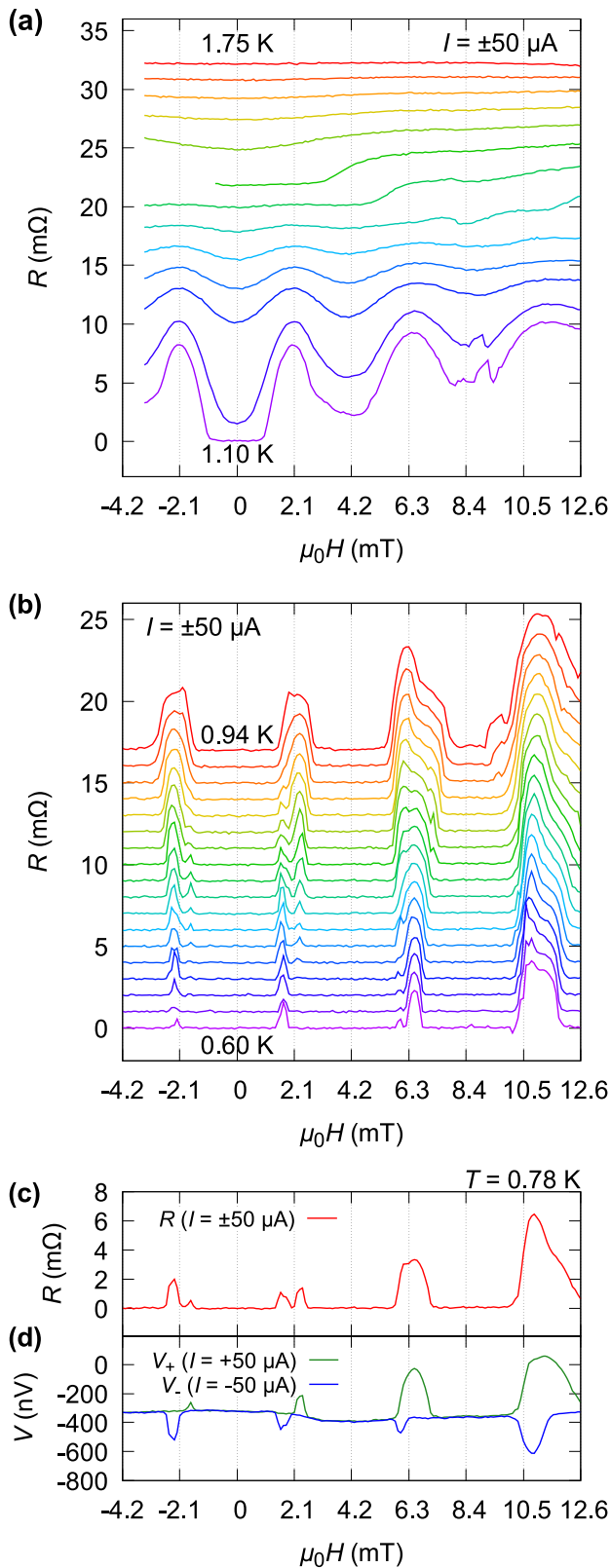
Fig. 5 Magnetotransport of Ring A. Magnetoresistance $R(H)$ with measurement current 50 μA for **a** temperatures between 1.75 and 1.10 K and **b** temperatures between 0.94 and 0.60 K. **c** $R(H)$ at 0.78 K. The I_c oscillations at this temperature are displayed in Fig. 4a. **d** The corresponding magnetovoltage when the measurement current is applied to one direction V_+ and to the other direction V_-. The peaks (dips) in V_+ (V_-) appear at different field values and hence double peaks appear in the resistance.

oscillations are completely absent in Ring C. Instead, for all temperature below T_c, we only observe a monotonous decay of $I_c(H)$. We find the lack of Josephson junctions to be a common characteristic among structures with a dominant extrinsic phase. A further example of this is given in Ring D (Supplementary Note 3 and Supplementary Fig. 4).

DISCUSSION

Before adopting ChDW scenario as the origin of the observed I_c oscillations, we consider other known mechanisms for I_c oscillations. Firstly, even in a homogeneous loop SQUID-like behaviour may emerge depending on the size of the ring with respective to either the penetration depth λ or the coherence length ξ. I_c can be modulated by the circulating persistent current I_p, which varies linearly with the flux, and switches its direction at every increment of $\Phi_0/2$. This mostly results in a sawtooth-like modulation of I_c[31], which cannot account for non-linear form of the patterns shown in Fig. 4. Furthermore, the magnitude of I_p is inversely proportional to the kinetic inductance L_K, which depends on the penetration depth $L_K \propto \lambda^2(T)$. If the I_c oscillations were driven by circulating currents, their amplitude ΔI_c would grow larger by lowering the temperature since $\Delta I_c \propto I_p \propto 1/\lambda^2(T)$[31]. This is clearly not the case for the Sr_2RuO_4 rings, where oscillation amplitude is unaffected by temperature (e.g. $\Delta I_c \approx 12$ μA at both temperatures shown in Fig. 4a). SQUID oscillations can also emerge in loops without weak link, if the dimensions are much smaller than $\xi(T)$ and $\lambda(T)$[32]. However, this is not applicable to our structures, where the radii and the width of the arms are several times larger than the characteristic length scales for $T \ll T_c$ (e.g. for Ring A, $\xi(T) \sim 0.07$ μm and $\lambda(T) \sim 0.19$ μm at $T = 0.78$ K).

Secondly, Cai et al. attributed the large-amplitude magnetoresistance of their Sr_2RuO_4 rings to current-excited moving vortices[28,29]. As demonstrated by Berdiyorov et al.[33], this mechanism can only produce large-amplitude oscillations over a finite temperature range, typically down to $T \sim 0.95T_c$ (e.g. see Fig. 6b of ref. [33] and Fig. 2 of ref. [34]). This is not the case for the Sr_2RuO_4 rings that are in the intrinsic (1.5-K) phase, as the magnetoresistance oscillations appear for all $T < T_c$ (see Fig. 5a, b and Fig. 3a in ref. [28]).

Thirdly, geometrical constrictions (e.g. bridges and nanowires) can serve as Josephson junctions, as long as their dimensions are comparable to ξ. The current-phase relation (CPR) of such junctions is defined by the ratio of $\xi(T)$ to the length of the weak link L. Since $\xi(T)$ varies with temperature while L remains fixed, the CPR of such weak links is strongly temperature dependent. Generally, lowering the temperature transforms the CPR from sinusoidal to a sawtooth-like function, which ultimately turns into multivalued relations once $L \geq 3.5\xi(T)$, corresponding to the nucleation of phase-slip centres[35–37]. The multivalued CPR manifests itself as a hysteretic $V(I)$ relation, which is a well-known characteristic of constriction junctions at $T \ll T_c$[38,39]. This is in direct contrast to the $V(I)$ curves of the Sr_2RuO_4 rings, which show negligible hysteresis for temperatures as low as $0.2T_c$ (see Fig. 2c). Furthermore, the interference patterns taken at over wide range of temperatures show the same overall shape, with characteristically round lobes (Fig. 4). This could not be produced by constriction junctions, as the interference pattern would be heavily deformed by the pronounced changes in $\xi(T)/L$ with temperature. In case of ChDWs, however, the length of the junction barrier is determined by the coherence length and therefore has a temperature dependence similar to $\xi(T)$. Hence, a ChDW junction can maintain a relatively fixed $\xi(T)/L(T)$ ratio for different temperatures. This would agree with the lack of hysteresis in our $V(I)$ measurements (Fig. 2c) and the unperturbed shape of the interference patterns (Fig. 4).

Lastly, we exclude the possibility of forming accidental proximity junctions by Ru inclusions or any other normal metal
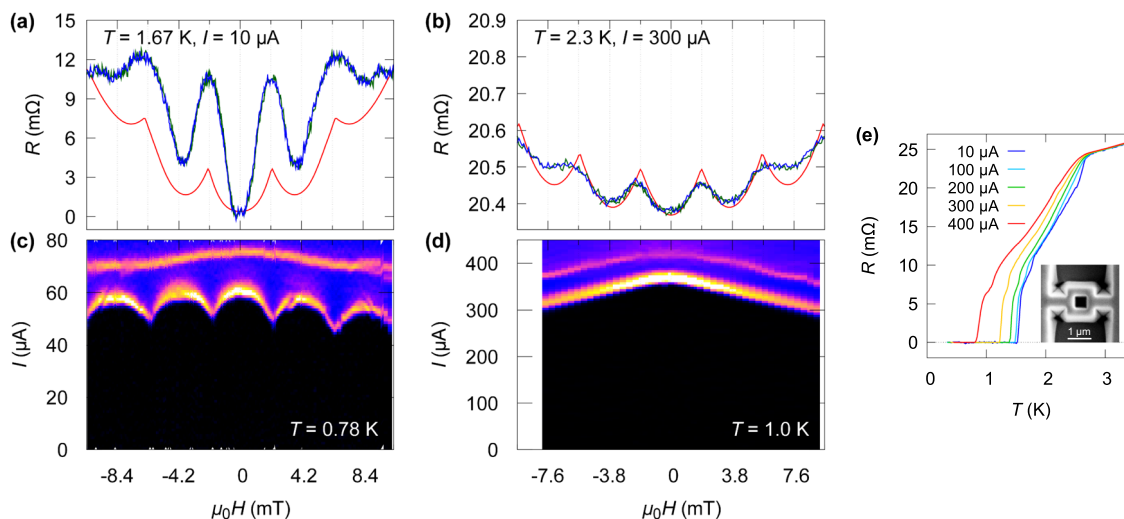
Fig. 6 Comparison with a ring that exhibits the Little–Parks (LP) oscillations. a Magnetoresistance $R(H)$ of Ring A near the transition temperature. **b** $R(H)$ of Ring C. The amplitude of the observed oscillations (blue and green) in Ring A is much greater than the expectation for the LP oscillations (red). In contrast, the observed oscillations in Ring C are in good agreement with a simulation for the LP oscillations. Colour maps of the differential resistance dV/dI of **c** Ring A and **d** Ring C as functions of magnetic field and measurement current. The bright part corresponds to the critical current. The critical current of Ring C does not show any oscillation. **e** Resistance as a function of temperature of Ring C. The onset T_c is 2.7 K, and hence the ring is in the extrinsic phase, which we consider as a non-chiral state. Data for panels (**b**) and (**e**) are adopted from ref. [27].

within the Sr_2RuO_4 crystal. Apart from their absence in the SEM images taken while the milling of the rings, inclusions would induce an extrinsic 3-K phase. The crystals, however, show no such enhancement of T_c either before or after FIB processing. Moreover, the (single) sharp resistive transitions of Rings A and B could not be produced in the presence of normal metal weak links. Accidental tunnel junctions, formed by nanocracks or grain boundaries, can also be excluded due to the high metallicity of our samples. In summary, the Josephson effect found in Sr_2RuO_4 microrings cannot be attributed to conventional types of weak link such as constriction junctions, kinematic vortices (phase-slip lines), proximity and tunnel junctions.

To summarise, our simulations of a chiral p-wave order parameter show that a mesoscopic loop with nanostructured transport leads can host a multi-domain state. The degenerate chiral states are separated by ChDWs located in the arms of the ring, where a pair of parallel Josephson junctions is formed due to the local suppression of both chiral states. We examined the existence of such junctions by performing transport experiments on Sr_2RuO_4 microrings. The rings with a sharp transition near 1.5 K show distinct I_c oscillations, similar to that of a DC SQUID with a pair of Josephson junctions with matching I_c. The junctions emerge together with the superconducting transition and are present for all temperatures below T_c. In contrast, for Sr_2RuO_4 rings with an extrinsic (3-K) phase, the Josephson junctions are entirely absent. Such rings show standard Little–Parks oscillations near T_c, which can be properly modelled, but no critical current oscillations. Our findings suggest that the Josephson junctions are an inherent property of the order parameter, and make a compelling case for the existence of ChDWs in the intrinsic (1.5-K) phase of Sr_2RuO_4. We should note that our present results formally do not distinguish the type of degenerate states responsible for the formation of the junctions; our transport measurements would also be consistent with domain walls of helical states, as well as of spin-singlet chiral states. This work also demonstrates that the combination order parameter simulations with mesoscopic structures can be instrumental in the study of superconducting domains and will, in coming experiments, allow for detailed

design and understanding of a system before the actual fabrication.

METHODS

Microring fabrication

Sr_2RuO_4 single crystals were prepared with the floating zone method[23], and their transition temperature T_c before the sample fabrication was confirmed to be 1.50 K using a compact AC susceptometer[40] in a Quantum Design PPMS. We crush the crystal into small pieces to obtain thin crystals with the thickness of approximately 1 μm. Although Sr_2RuO_4 is chemically stable in the ambient condition, we find that small crystals can degrade in the air. Therefore, freshly crushed crystals were used. The crystal is placed on a $SrTiO_3$ substrate, where it is contacted by either gold or silver for transport measurements. For Rings A, C and D, two pads of high-temperature-cure silver paint (6838, Dupont) are attached to the two sides of the crystal. The paint is then cured at 500 °C for 20 min. In case of Rings B and E however, the crystals are contacted using a combination of electron-beam lithography and sputter deposition of gold. Once a crystal is contacted by the gold or silver paint, a 100-nm-thick layer of SiO_2 is deposited using electron beam evaporation to protect the crystal during structuring. The contacts and the crystal underneath are then cut with a Gallium FIB to produce a four-wire arrangement. Lastly, the microrings are structured using the FIB (30 kV, 20 pA).

Measurements

Transport measurements were performed in a ^{3}He refrigerator (Heliox, Oxford Instruments) down to 0.3 K. In the DC resistance measurement, we flip the direction of the measurement current to subtract the contribution of the thermoelectric voltage, and the resistance R is defined to be $R = [V(I) - V(-I)]/2I$. The transition temperature shift due to the LP oscillations is calculated to be approximately 10 mK by using Eq. (1). Therefore, temperature stability during the magnetoresistance measurement must be much smaller than this value. By putting a 80-Ω by-pass resister in parallel to the heater and by tuning the PID values of the temperature controller, we achieved a temperature stability of 100 μK. Current–voltage $V(I)$ measurements are performed under constant temperature and magnetic field with triangular current waves of frequency 2 mHz.

Simulations

For details of the Ginzburg–Landau simulations, we refer to the formalism of ref. [20], and the additional discussion in the Supplementary information.

DATA AVAILABILITY

The data that support the findings of this study are available from the corresponding author upon reasonable request.

REFERENCES

1. Mackenzie, A. & Maeno, Y. The superconductivity of Sr_2RuO_4 and the physics of spin-triplet pairing. *Rev. Mod. Phys.* **75**, 657–712 (2003).
2. Maeno, Y., Kittaka, S., Nomura, T., Yonezawa, S. & Ishida, K. Evaluation of the spin-triplet superconductivity in Sr_2RuO_4. *J. Phys. Soc. Jpn.* **81**, 011009 (2012).
3. Rice, T. M. & Sigrist, M. Sr_2RuO_4: an electronic analogue of ^{3}He. *J. Phys. Cond. Mat.* **7**, L643–L648 (1995).
4. Luke, G. et al. Time reversal symmetry breaking superconductivity in Sr_2RuO_4. *Nature* **391**, 558–561 (1998).
5. Xia, J., Maeno, Y., Beyersdorf, P. T., Fejer, M. M. & Kapitulnik, A. High resolution polar Kerr effect measurements of Sr_2RuO_4: evidence for broken time reversal symmetry in the superconducting state. *Phys. Rev. Lett.* **97**, 167002 (2006).
6. Pustogow, A. et al. Constraints on the superconducting order parameter in Sr_2RuO_4 from oxygen-17 nuclear magnetic resonance. *Nature* **574**, 72–75 (2019).
7. Ishida, K., Manago, M., Kinjo, K. & Maeno, Y. Reduction of the ^{17}O Knight shift in the superconducting state and the heat-up effect by NMR pulses on Sr_2RuO_4. *J. Phys. Soc. Jpn.* **89**, 034712 (2020).
8. Ivanov, D. A. Non-Abelian statistics of half-quantum vortices in *p*-wave superconductors. *Phys. Rev. Lett.* **86**, 268–271 (2001).
9. Das Sarma, S., Nayak, C. & Tewari, S. Proposal to stabilize and detect half-quantum vortices in strontium ruthenate thin films: non-Abelian braiding statistics of vortices in a $p_x + ip_y$ superconductor. *Phys. Rev. B* **73**, 220502(R) (2006).
10. Nayak, C., Simon, S. H., Stern, A., Freedman, M. & Das Sarma, S. Non-Abelian anyons and topological quantum computation. *Rev. Mod. Phys.* **80**, 1083–1159 (2008).
11. Mackenzie, A. P., Scaffidi, T., Hicks, C. W. & Maeno, Y. Even odder after twenty-three years: the superconducting order parameter puzzle of Sr_2RuO_4. *npj Quantum Mater.* **2**, 40 (2017).
12. Anwar., M. S. et al. Y. Anomalous switching in $Nb/Ru/Sr_2RuO_4$ topological junctions by chiral domain wall motion. *Sci. Rep.* **3**, 2480 (2013).
13. Kidwingira, F., Strand, J. D., van Harlingen, D. J. & Maeno, Y. Dynamical superconducting order parameter domains in Sr_2RuO_4. *Science* **314**, 1267–1271 (2006).
14. Maeno, Y. et al. Enhancement of superconductivity of Sr_2RuO_4 to 3 K by embedded metallic microdomains. *Phys. Rev. Lett.* **81**, 3765–3768 (1998).
15. Kittaka, S., Yaguchi, H. & Maeno, Y. Large enhancement of 3-K phase superconductivity in the Sr_2RuO_4–Ru eutectic system by uniaxial pressure. *J. Phys. Soc. Jpn.* **78**, 103705 (2009).
16. Anwar, M. S. et al. Multicomponent order parameter superconductivity of Sr_2RuO_4 revealed by topological junctions. *Phys. Rev. B* **95**, 224509 (2017).
17. Steppke, A. et al. Strong peak in T_c of Sr_2RuO_4 under uniaxial pressure. *Science* **355**, eaaf9398 (2017).
18. Wang, J. et al. Anomalous magnetic moments as evidence of chiral superconductivity in a Bi/Ni bilayer. *Phys. Rev. B* **96**, 054519 (2017).
19. Sigrist, M. & Agterberg, D. F. The role of domain walls on the vortex creep dynamics in unconventional superconductors. *Progr. Theor. Phys.* **102**, 965–981 (1999).
20. Fernández Becerra, V. & Milošević, M. V. Multichiral ground states in mesoscopic *p*-wave superconductors. *Phys. Rev. B* **94**, 184517 (2016).
21. Zhang, L.-F., Covaci, L. & Milošević, M. V. Topological phase transitions in small mesoscopic chiral *p*-wave superconductors. *Phys. Rev. B* **96**, 224512 (2017).
22. Little, W. A. & Parks, R. D. Observation of quantum periodicity in the transition temperature of a superconducting cylinder. *Phys. Rev. Lett.* **9**, 9–12 (1962).
23. Mao, Z. Q., Maeno, Y. & Fukazawa, H. Crystal growth of Sr_2RuO_4. *Mater. Res. Bull.* **35**, 1813–1824 (2000).
24. Vaglio, R., Attanasio, C., Maritato, L. & Ruosi, A. Explanation of the resistance-peak anomaly in nonhomogeneous superconductors. *Phys. Rev. B* **47**, 15302 (1993).
25. Ginzburg, V. L. Some remarks concerning the macroscopic theory of superconductivity. *Sov. Phys. JETP* **3**, 621–623 (1956).
26. Müller, A., Milošević, M. V., Dale, S. E., Engbarth, M. A. & Bending, S. J. Magnetization measurements and Ginzburg–Landau simulations of micron-size β-tin

samples: evidence for an unusual critical behavior of mesoscopic type-I superconductors. *Phys. Rev. Lett.* **109**, 197003 (2012).
27. Yasui, Y. et al. Little-Parks oscillations with half-quantum fluxoid features in Sr_2RuO_4 microrings. *Phys. Rev. B* **96**, 180507(R) (2017).
28. Cai, X., Ying, Y. A. & Staley, N. E. Unconventional quantum oscillations in mesoscopic rings of spin-triplet superconductor Sr_2RuO_4. *Phys. Rev. B* **87**, 081104(R) (2013).
29. Cai, X. et al. Magnetoresistance oscillations and the half-flux-quantum state in spin-triplet superconductor Sr_2RuO_4. Preprint at https://arxiv.org/abs/1507.00326v2 (2016).
30. Moshchalkov, V. V. et al. Effect of sample topology on the critical fields of mesoscopic superconductors. *Nature* **373**, 319–322 (1995).
31. Michotte, S., Lucot, D. & Mailly, D. Fluxoid quantization in the critical current of a niobium superconducting loop far below the critical temperature. *Phys. Rev. B* **81**, 100503 (2010).
32. Fink, H. J., Grünfeld, V. & López, A. Quantum-interference device without Josephson junctions. *Phys. Rev. B* **35**, 35 (1987).
33. Berdiyorov, G. R. et al. Large magnetoresistance oscillations in mesoscopic superconductors due to current-excited moving vortices. *Phys. Rev. Lett.* **109**, 057004 (2012).
34. Sochnikov, I., Shaulov, A., Yeshurun, Y., Logvenov, G. & Božović, I. Large oscillations of the magnetoresistance in nanopatterned high-temperature superconducting films. *Nat. Nanotechnol.* **5**, 516–519 (2012).
35. Golubov, A. A., Kupriyanov, M. Y. & Il'Ichev, E. The current-phase relation in Josephson junctions. *Rev. Mod. Phys.* **76**, 411 (2004).
36. Troeman, A. G. P. et al. Temperature dependence measurements of the supercurrent-phase relationship in niobium nanobridges. *Phys. Rev. B* **77**, 024509 (2008).
37. Sivakov, A. G., Pokhila, A. S., Glukhov, A. M., Kuplevakhsky, S. V. & Omelyanchouk, A. N. Oscillations of critical superconducting current in thin doubly-connected Sn films in an external perpendicular magnetic field. *J. Low. Temp. Phys.* **40**, 408 (2014).
38. Hazra, D., Pascal, L. M., Courtois, H. & Gupta, A. K. Hysteresis in superconducting short weak links and μ-SQUIDs. *Phys. Rev. B* **82**, 184530 (2010).
39. Kumar, N., Fournier, T., Courtois, H., Winkelmann, C. B. & Gupta, A. K. Reversibility of superconducting Nb weak links driven by the proximity effect in a quantum interference device. *Phys. Rev. Lett.* **114**, 157003 (2015).
40. Yonezawa, S., Higuchi, T., Sugimoto, Y., Sow, C. & Maeno, Y. Compact ac susceptometer for fast sample characterization down to 0.1 K. *Rev. Sci. Instrum.* **86**, 093903 (2015).

AUTHOR CONTRIBUTIONS

The crystals were grown in the group of Y.M. at Kyoto University. K.L., Y.Y., R.F., and T.T. FIB-structured the crystals that were prepared by Y.Y. Y.Y., K.L., and R.F. performed the transport measurements. M.S.A. took part in the discussion. S.Y. and Y.M. supervised the measurements. Y.Y. and K.L. analysed the results. V.F.B. and M.V.M. carried out the TDGL simulations. Y.Y., K.L., V.F.B., S.Y., M.V.M., J.A., and Y.M. wrote the paper with inputs from all the authors. Y.Y. and K.L. contributed equally to this work.

COMPETING INTERESTS

The authors declare no competing interests.

ADDITIONAL INFORMATION

Supplementary information is available for this paper at https://doi.org/10.1038/s41535-020-0223-7.

Correspondence and requests for materials should be addressed to Y.M.